

Operator Lévy Flight: Light Cones in Chaotic Long-Range Interacting Systems

Tianci Zhou,^{1,*} Shenglong Xu,^{2,6} Xiao Chen,^{1,3} Andrew Guo,⁴ and Brian Swingle⁵

¹Kavli Institute for Theoretical Physics, University of California, Santa Barbara, California 93106, USA

²Condensed Matter Theory Center and Department of Physics, University of Maryland, College Park, Maryland 20742, USA

³Department of Physics and Center for Theory of Quantum Matter, University of Colorado, Boulder, Colorado 80309, USA

⁴Joint Center for Quantum Information and Computer Science and Joint Quantum Institute, NIST/University of Maryland, College Park, Maryland 20742, USA

⁵Condensed Matter Theory Center, Maryland Center for Fundamental Physics, Joint Center for Quantum Information and Computer Science, and Department of Physics, University of Maryland, College Park, Maryland 20742, USA

⁶Department of Physics & Astronomy, Texas A&M University, College Station, Texas 77843, USA



(Received 1 October 2019; revised manuscript received 20 November 2019; accepted 16 April 2020; published 4 May 2020)

We argue that chaotic power-law interacting systems have emergent limits on information propagation, analogous to relativistic light cones, which depend on the spatial dimension d and the exponent α governing the decay of interactions. Using the dephasing nature of quantum chaos, we map the problem to a stochastic model with a known phase diagram. A linear light cone results for $\alpha \geq d + 1/2$. We also provide a Lévy flight (long-range random walk) interpretation of the results and show consistent numerical data for 1D long-range spin models with 200 sites.

DOI: 10.1103/PhysRevLett.124.180601

Introduction.—Quantum information cannot propagate faster than light. However, in many laboratory settings, the speed of light is effectively infinite, since the natural dynamical timescales are long compared to the light-crossing time. Hence, these systems can sometimes be modeled as having instantaneous long-range interactions, for example, electric and magnetic dipolar interactions. Such nonlocal interactions potentially allow rapid information transfer between distant locations [1–5], making them attractive for quantum information processing.

Remarkably, short-range interaction enforces an emergent speed limit [6], even when the speed of light is effectively infinite. We study the analogous possibility of emergent limits on information propagation in long-range interacting systems. We refer to these limits as effective light cones even though their spacetime shape may not be that of a cone. Our focus is on power-law interactions that fall off with distance r as $r^{-\alpha}$ since these systems are common in the lab and their emergent light cones have been intensely studied [7–21]. Using the concepts and tools recently developed from the study of many-body quantum chaos [18,22–24], we argue that chaotic power-law interacting systems have a generic emergent light cone structure which depends only on α and the spatial dimension d .

We diagnose emergent light cones by studying the commutator of two operators, where one acts as the perturbation and the other probes whether the perturbation has spread beyond a given spacetime point. Such a commutator would exactly vanish outside the light cone in a *relativistic* model, whereas for quantum lattice systems without manifest Lorentz invariance, the commutator may

still be nonzero for arbitrarily small times. Furthermore, for long-range interacting systems, the region outside of which the commutator is small cannot in general be bounded by a simple, *linear* contour; the notion of a light cone is still applicable here, however, since information can hardly spread beyond the contour at a given point in time.

The key quantity is the expectation value of the squared commutator (closely related to the out-of-time-ordered correlator [25–27], or OTOC) defined (in our lattice setting, at infinite temperature) as

$$C(x, t) = \text{Tr}([W(t), V]^\dagger [W(t), V]) / \text{Tr}(\mathbb{I}), \quad (1)$$

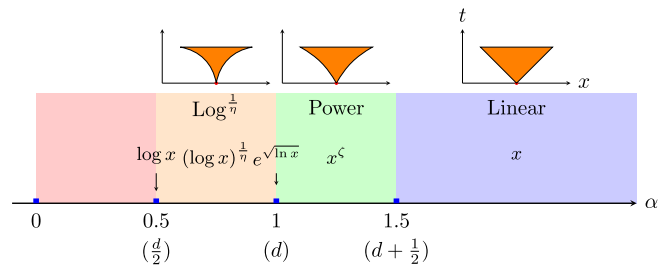


FIG. 1. The light cone (LC) contours of $C(x, t)$ in Model 1 [48,49]. The α axis marks the transition exponents in one dimension (d -dimensional data in the parenthetical). In order of increasing α , the light cone transitions from logarithmic to power law to linear. The scaling functions for $t_{\text{LC}}(x)$ in each phase as well as the marginal scalings at $\alpha = d/2$ and d are displayed. The exponents ζ and $1/\eta$ are given by $\zeta = 2\alpha - 2d$, $\eta = \log_2(d/\alpha)$. The power-law and linear light cone regimes are also numerically verified in chaotic long-range spin chains.

where $W(t) = e^{iHt} W e^{-iHt}$ is the Heisenberg form of the local operator W and V is another local operator a distance x away from W . Happily, these objects can be measured in experiment [28–39], including in large-scale systems with power-law interactions [40].

The emergent light cone is defined in terms of the spacetime contours determined by $C = \text{constant}$, as these track the effective spread of the perturbation in spacetime. For local quantum chaotic systems, one typically finds that the contours are asymptotically straight, independent of the precisely chosen contour, although in general there is a rich shape structure in the nonasymptotic regime. In the power-law case, Ref. [18] provided a systematic study of the light cone structure for systems with time-dependent random couplings. By random averaging, those authors gave strong numerical evidence for a complex light cone structure depending on α .

In this work, we propose that the phase diagram in Ref. [18] is generic for chaotic power-law interacting systems *even without randomness*. Specifically, we exclude systems with gauge or intrinsic constraints (see, e.g., Refs. [41,42]) that prevent ergodicity. Our theoretical picture is that dephasing in such systems due to quantum chaos leads to an effective stochastic description of the emergent light cone. The resulting effective model falls into the “long-range dispersal” class for which a universal phase diagram is known. We rigorously locate the phase boundaries that delineate the regions of ballistic, superballistic, and exponential growth (Fig. 1). Furthermore, we develop a novel numerical scheme for operator spreading using time-dependent variational principle in the matrix product representation (TDVP-MPO) [43–47]. As far as we know, it is the most efficient method to study the operator dynamics of large scale long-range systems so far, which enables us to simulate chaotic spin chains of up to 200 sites. The results are consistent with the phase diagram in Fig. 1.

Operator spreading.—In general, chaotic time evolution will increase the support and complexity of $W(t)$, a process known as operator spreading. We propose that due to dephasing, such processes can be approximated by a stochastic model that generates a universal phase diagram.

We use a height representation introduced in Refs. [18,24] to describe the operator spreading, but there are many other approaches [50–54]. In a 1D chain of spin- $\frac{1}{2}$ particles of length L , we expand $W(t)$ into Pauli string basis $\{B_\mu\}$:

$$W(t) = \sum_{\mu} a_{\mu}(t) B_{\mu}. \quad (2)$$

With the normalization $\text{tr}[W^\dagger(t)W(t)] = 1$, the coefficients $|a_{\mu}(t)|^2$ give a normalized probability distribution over $\{B_{\mu}\}$.

Each basis operator has a height as follows: the i th component h_i for operator B_{μ} is 0 if B_{μ} is identity on site i and 1 otherwise. Together these h_i form an L -component vector $\mathbf{h} \in \{0, 1\}^L$. The height representation does not distinguish different Pauli operators, so many operators

have the same height. If the distribution over operators of a given height \mathbf{h} is more-or-less random, then the chaotic operator dynamics is succinctly represented by the height probability distribution $f(\mathbf{h}, t) = \sum_{\text{height}(B_{\mu})=\mathbf{h}} |a_{\mu}(t)|^2$. Since the commutator $[W(t), V]$ can only be nonzero if $W(t)$ is not the identity at the location of V , it follows that $C(x, t)$ is proportional to the *mean height* of $W(t)$ at site x (again provided the distribution over operators of a given height is uniform).

The distribution f is defined on the space of 2^L height states. We refer to sites with $h_i = 1$ as occupied, and otherwise as unoccupied. Initially, a simple local operator $W(0)$ only has one site occupied and the distribution f is concentrated on that height vector. Time evolution generally expands the operator, and the height distribution is correspondingly spread over more height configurations. Because of the decaying strength of the interaction, sites closer to $W(0)$ are more likely to increase their height earlier. As a result, the dynamics of the height distribution encodes the light cone structure.

The height picture is particularly useful for chaotic systems because their pseudorandom character implies that the evolution of $f(\mathbf{h}, t)$ is often approximately Markovian. This observation has been made in local systems [23,50–53], where an additional site can become occupied only if it is next to an occupied site.

We postulate the following effective Markovian transition rates for the f dynamics. For definiteness, suppose the Hamiltonian is $H = \sum_{\nu} J_{\nu} H_{\nu}$, where the H_{ν} are Pauli strings with nonidentity elements on only two sites a distance $r(H_{\nu})$ apart and the couplings J_{ν} scales as $r(H_{\nu})^{-\alpha}$. If the model is chaotic, then it will exhibit an effective loss of coherence on a timescale τ_{coh} . The Markovian transition rates are then estimated to be of order $J_{\nu}^2 \tau_{\text{coh}} \propto r^{-2\alpha}$, which leads to a probability of jumping from the top to the bottom configuration in Fig. 2(a). Hence, the stochastic height dynamics of Model 1 is (1) Initially only one site is occupied. (2) Each occupied site contributes a transition rate proportional to $r^{-2\alpha}$ to occupy an empty site a distance r away.

The effective dephasing and the stochastic rate estimate above are our key assumptions to understanding the light cone structure. The resulting Model 1 can be *exactly* realized in an idealized model called a Brownian circuit [18,24,54], where the couplings are Brownian motions. Here, we believe the assumed randomness of chaos can effectively do the same job leading to Model 1.

As discussed above, we define the light cone structure by studying its level sets of the squared commutator. The curve parametrized by $t = t_{\text{LC}}(x)$ with $C[x, t_{\text{LC}}(x)] = \epsilon$ defines the light cone contour with threshold ϵ , which is expected to depend strongly on α . In the local limit, $\alpha \rightarrow \infty$, the leading behavior is $t_{\text{LC}}(x) \sim x$, i.e., a linear light cone. When $\alpha = 0$, Model 1 completely loses locality, and $t_{\text{LC}}(x) \rightarrow 0$ in an infinite chain. The general phase diagram

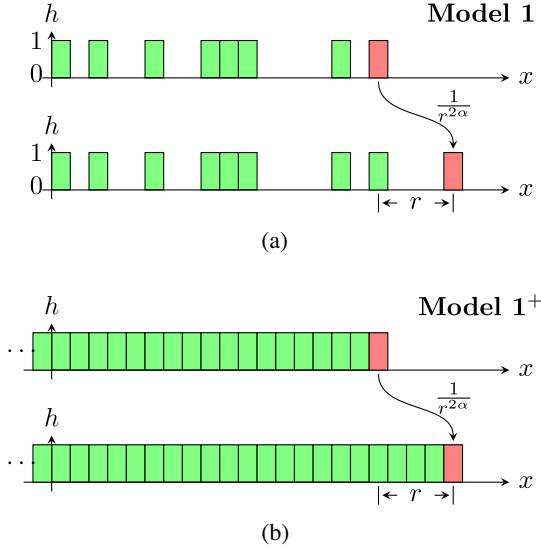


FIG. 2. Model 1 and a faster Model 1⁺. Filled rectangles are occupied sites. (a) Each of them (red on the top) contributes a rate proportional to $r^{-2\alpha}$ to occupy an empty site (red on the bottom) with distance r . (b) Make the same transition and then fill all the sites on its left.

has been obtained exactly in Refs. [48,49]; translating it to our setting yields Fig. 1.

There are four different phases characterized by different light cone scalings. In one dimension, $\alpha < 0.5$ is the completely nonlocal phase. The transition occurs at the threshold below which the jump rate $\sim r^{-(2 \times 0.5)}$ in Model 1 becomes un-normalizable in an infinite chain. On a finite chain, the operator spreading is similar to that of the Sachdev-Ye-Kitaev model [18,24,26,55,56]. As α increases, one finds a phase with $t_{\text{LC}}(x) \sim (\log x)^{1/\eta}$ ($0 < \eta \leq 1$) for $0.5 \leq \alpha < 1$ and a power-law light cone phase for $1 < \alpha < 1.5$. Finally, when $\alpha \geq 1.5$, a linear light cone emerges.

A faster model: Model 1⁺.—To better understand these results, and to learn more about the shape of the contours, we study an even simpler model that still captures much of the physics. We dub it “Model 1⁺” and illustrate in Fig. 2(b). Its modified transition rule is 2’ Make a transition (as in Model 1) and then fill in all the empty sites “behind” the newly occupied site.

Clearly, Model 1⁺ spreads faster than Model 1, so its value for $C(x, t)$ will upper bound that of Model 1. However, Model 1⁺ is simpler to analyze because its state is completely determined by the motion of the outermost point, thus reducing it to a single particle problem. In one dimension, the dynamics can be sped up by taking all the sites with $x \leq 0$ to be occupied in the initial height state. The motion of the outermost point becomes Markovian, and the rate to move forward r sites is then $\sum_{r'=-\infty}^r (r')^{-2\alpha} \sim r^{1-2\alpha}$.

Such a long-range random walk is called a Lévy flight (see Refs. [57–59]), where the displacement of each jump

X_t (at time t) is an independent random variable with distribution $f_{\text{jump}}(x)$ that scales as $x^{-(1+\alpha_{\text{Lévy}})}$ when $x \rightarrow \infty$. According to the generalized central limit theorem [60], the total displacement will converge to a Lévy stable distribution $L_{\alpha_{\text{Lévy}}, \beta_{\text{Lévy}}}$, with parameter $\alpha_{\text{Lévy}} = 2\alpha - 2$ and $\beta_{\text{Lévy}} = 1$ for the present case. The distribution for the right-most occupied site $\rho(r, t)$ scales as

$$\rho(x, t) \sim \begin{cases} L_{2\alpha-2,1}(x/t^{1/\zeta}) & 1 < \alpha \leq 1.5, \\ L_{2\alpha-2,1}((x - v_B t)/t^{1/\zeta}) & 1.5 < \alpha < 2, \\ \exp(-(x - v_B t)^2/2Dt) & 2 \leq \alpha, \end{cases} \quad (3)$$

where $L_{\alpha,\beta}$ is the Lévy stable distribution $\zeta = 2\alpha - 2$ and v_B and D are the first and second moments of $f_{\text{jump}}(x)$ when they exist. The probability for site x to be occupied is equal to $\int_x^\infty \rho(x', t) dx'$ in Model 1⁺, which leads to the light cones in the second column of Table I:

The transition points $\alpha = 1, 1.5$ and 2 are the critical values above which the jump distribution $f_{\text{jump}}(x)$ of Model 1⁺ starts to be normalizable and acquires mean velocity v_B and variance D , respectively. In the following, we review the quantitative predictions on Model 1 by Model 1⁺. Aside from the light cone scalings and characteristic width, we also study the wavefronts’ spatial dependences at fixed time. We refer to the large- x limit of $C(x, t)$ at fixed t as the *tail*. For small t in Model 1, the tail should be roughly equal to the probability of a rare jump from the initial seed at site 0, i.e., as $x^{-2\alpha}$. The tails we discuss are for large t .

From Table I, all the scalings about the light cones are identical for both models when $\alpha \geq 1.5$. In this regime, Model 1⁺ has a linear light cone and since it spreads faster than Model 1, the later must also have a linear light cone. We would further expect Model 1 to form a domain of occupied sites within the light cone, rendering the two models qualitatively similar. In particular the widths of $t^{1/(2\alpha-2)}$ and \sqrt{t} have been verified in the classical simulation of Model 1 [60].

When $1 < \alpha < 1.5$, Model 1⁺ has a power-law light cone, whereas that of Model 1 could potentially be more restrictive. But suppose Model 1 were to have a linear light cone; then a domain of occupied sites would form, so that

TABLE I. Scalings of light cone, its broadening (width), and tail of Model 1⁺ and comparison with Model 1.

	Model 1 ⁺			Model 1		
α	LC	Width	Tail	LC	Width	Tail
[0.5, 1)	N/A	N/A	N/A	$e^{t \log_2(1/\alpha)}$	N/A	$x^{-2\alpha}$
$(1, \frac{3}{2})$	$t^{1/(2\alpha-2)}$	N/A	$x^{-(2\alpha-2)}$	$t^{1/(2\alpha-2)}$	N/A	
$(\frac{3}{2}, 2)$	$v_B t$	$t^{1/(2\alpha-2)}$		$v_B t$	$t^{1/(2\alpha-2)}$	$x^{-(2\alpha-2)}$
2		$(t \ln t)^{1/2}$	Gaussian		$(t \ln t)^{1/2}$	Gaussian
$(2, \infty)$		$t^{1/2}$			$t^{1/2}$	

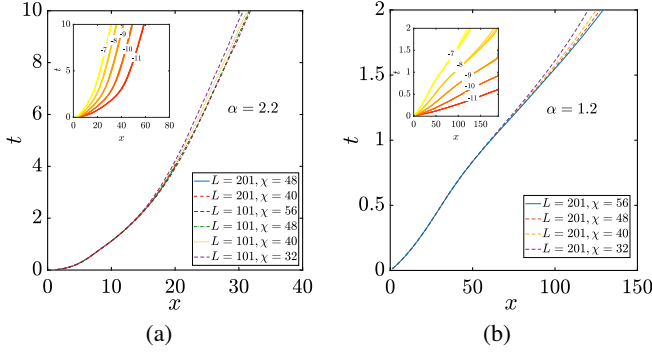


FIG. 3. The light cone of the long-range mixed-field Ising model for (a) $\alpha = 2.2$ and (b) $\alpha = 1.2$. Contours of $C(x, t)$ at threshold $\epsilon = e^{-7}$ are the main figures and other thresholds in the insets. Various system sizes and bond dimensions confirm convergence.

the light cone of Model 1 would be identical to that of Model 1⁺. But the latter has faster-than-linear propagation, leading to a contradiction. In practice, Model 1 has the same light cone scaling as Model 1⁺ [48,49], but the gaps between filled sites in Model 1 gives a different tail scaling than Model 1⁺. Within a mean-field approximation [60], we find the tail scaling to be $x^{-2\alpha}$, which is further numerically verified in Model 1 and a long-range spin chain discussed below.

Finally, when $\alpha < 1$, the long-range jumps of Model 1 create large gaps between the occupied sites. The approximation of a solid domain as in Model 1⁺ does not work, and the problem is many body in nature.

We briefly comment on the situation in higher dimensions. The transition rate $r^{-\alpha}$ is normalizable in d dimension only when $\alpha > d/2$. When we consider the corresponding Model 1⁺, the outermost point jumps with rate $\int d^d r r^{-2\alpha} \sim r^{-2\alpha+d}$. The existence of the zeroth, first, and second moments gives the general transition points marked in Fig. 1.

Numerical results.—We test the dephasing mechanism and other predictions mentioned above in a long-range mixed field Ising model with Hamiltonian

$$H = -\sum_{r,r'} \frac{J}{|r-r'|^\alpha} \sigma_r^z \sigma_{r'}^z - \sum_r h_z \sigma_r^z - \sum_r h_x \sigma_r^x, \quad (4)$$

where J is set to 1 as the energy unit, and the fields h_z and h_x are set to 0.5 and 1.05, respectively.

We implement the TDVP algorithm in operator space, which treats the operator as a matrix-product state and optimizes within the space of matrix-product representations [43,44,61]. The “super” Hamiltonian $\mathcal{H} = H \otimes I - I \otimes H^*$ of the long-range interaction is explicitly constructed and fed into the state-based TDVP algorithm [44]. We expect that information far ahead of the wave front can

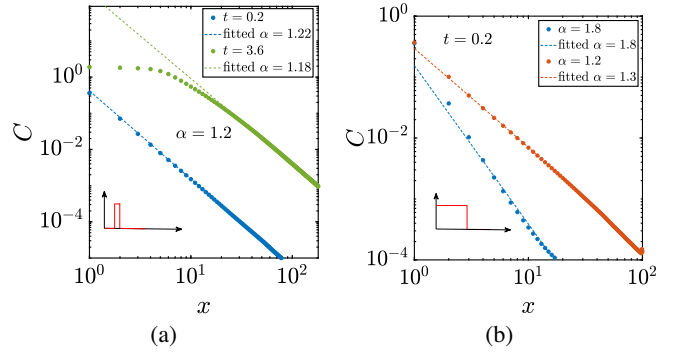


FIG. 4. Tail of the front for (a) a point and (b) domain wall initial conditions. (a) At $\alpha = 1.2$, the decay fits $x^{-2\alpha}$ at long times. (b) The short time decay fits $C = a(x^{1-2\alpha_{\text{fitted}}} - (x + x_0)^{1-2\alpha_{\text{fitted}}})$, where x_0 is the domain wall length. $\alpha_{\text{fitted}} \approx \alpha$, confirming the Lévy flight prediction.

be extracted with relatively low bond dimension, enabling us to simulate up to 200 sites.

In Fig. 3, we present the contour plots of $C(x, t)$ for $\alpha = 2.2$ and $\alpha = 1.2$, which demonstrate the linear and power-law light cones, respectively. The insets show the contours for different values of the threshold, ϵ . Equation (3) predicts that the contours will follow the relations $(x - v_B t)/\sqrt{t} \sim \text{const}$ and $x \sim t^{1/5}$ for the linear and power-law light cones, respectively. The former gives convex curves that become parallel asymptotically, while the latter gives concave curves that disperse. These features are reflected in Figs. 3(a) and 3(b).

A precise verification of the phase boundary is computationally challenging. We instead measure the spatial dependence of the power-law tail to verify the proposed dephasing scheme. Figure 4(a) shows the tail of the front for a point initial condition with $\alpha = 1.2$. The decay exponent remains close to 2α even at late times, consistent with the mean field argument [60]. In contrast, a domain wall initial condition with $h = 1$ for $x < 0$ will generate a tail that scales as $x^{-2\alpha-1}$ at early times. In Fig. 4(b), we fit the decay while taking into account the finite size of the domain and show that the fitting parameter α_{fitted} is fairly close to α .

Discussion and conclusion.—We studied information propagation in chaotic long-range interacting systems via an analysis of the light cone structure of the squared commutator. Invoking a dephasing mechanism, we proposed a general phase diagram for such chaotic systems that generalizes the one proposed in Ref. [18] that exhibits logarithmic, power-law, and linear light cone regimes. In particular, we analytically compute and numerically confirm the emergence of a linear light cone when the power-law exponent of the interaction strength $\alpha \geq 1.5$. The powerful TDVP-MPO algorithm allows us to simulate systems with 200 sites, so that pertinent results at late times can be explicitly verified.

A further simplification of the model yields a simple Lévy flight picture (Model 1⁺) that describes the operator spreading in generic long-range interacting systems. It is remarkable that we can determine all the phase transition points at where the moments of Lévy flight diverge, as well as the OTOC scaling close to the light cone. Both Model 1 and the associated arguments are also generalizable to systems with a large number of on-site degrees of freedom, which we leave to future work.

Recently, Ref. [20] proved a general Lieb-Robinson-type bound with a linear light cone for $\alpha > 3$ in one dimension. We here have a smaller threshold at $\alpha = 1.5$. This is in accordance with folklore that chaos usually prevents an optimal rate of propagation. Thus, we anticipate that the critical α for the systems we consider will generally be smaller than those of theoretical bounds.

We acknowledge insightful discussions with Minh Tran and especially Sarang Gopalakrishnan for pointing out the relevance to the Lévy flight at very early stage of the project. We also thank the accommodation and interactive environment of the KITP program “The Dynamics of Quantum Information” and the Aspen winter conference “Many-Body Quantum Chaos.” X. C. and T. Z. are supported by postdoctoral fellowships from the Gordon and Betty Moore Foundation, under the EPIQS initiative, Grant No. GBMF4304, at the Kavli Institute for Theoretical Physics. X. C. acknowledges support from DARPA DRINQS program. This research is supported in part by the National Science Foundation under Grant No. NSF PHY-1748958. We acknowledge support from the Center for Scientific Computing from the CNSI, MRL: an NSF MRSEC (DMR-1720256) and NSF CNS-1725797, University of Maryland supercomputing resources and advanced computing resources provided by Texas A&M High Performance Research Computing. S. X. and B. S. acknowledge support from the U.S. Department of Energy, Office of Science, Advanced Scientific Computing Research Quantum Algorithms Teams program as part of the QOALAS collaboration. A. Y. G. is supported by the NSF Graduate Research Fellowship Program under Grant No. DGE-1840340. A. Y. G. also acknowledges partial support by the DOE ASCR Quantum Testbed Pathfinder program (Award No. DE-SC0019040), DOE BES QIS program (Award No. DE-SC0019449), NSF PFCQC program, AFOSR, ARO MURI, ARL CDQI, and NSF PFC at JQI.

*tzhou@kitp.ucsb.edu

- [1] A. Y. Guo, M. C. Tran, A. M. Childs, A. V. Gorshkov, and Z.-X. Gong, *arXiv:1906.02662*.
- [2] N. Lashkari, D. Stanford, M. Hastings, T. Osborne, and P. Hayden, *J. High Energy Phys.* **04** (2013) 022.
- [3] Z. Eldredge, Z.-X. Gong, J. T. Young, A. H. Moosavian, M. Foss-Feig, and A. V. Gorshkov, *Phys. Rev. Lett.* **119**, 170503 (2017).
- [4] G. Gualdi, V. Kostak, I. Marzoli, and P. Tombesi, *Phys. Rev. A* **78**, 022325 (2008).
- [5] M. Avellino, A. J. Fisher, and S. Bose, *Phys. Rev. A* **74**, 012321 (2006).
- [6] E. H. Lieb and D. W. Robinson, *Commun. Math. Phys.* **28**, 251 (1972).
- [7] D. Porras and J. I. Cirac, *Phys. Rev. Lett.* **92**, 207901 (2004).
- [8] M. B. Hastings and T. Koma, *Commun. Math. Phys.* **265**, 781 (2006).
- [9] J. W. Britton, B. C. Sawyer, A. C. Keith, C. C. J. Wang, J. K. Freericks, H. Uys, M. J. Biercuk, and J. J. Bollinger, *Nature (London)* **484**, 489 (2012).
- [10] R. Blatt and C. F. Roos, *Nat. Phys.* **8**, 277 (2012).
- [11] B. Yan, S. A. Moses, B. Gadway, J. P. Covey, K. R. A. Hazzard, A. M. Rey, D. S. Jin, and J. Ye, *Nature (London)* **501**, 521 (2013).
- [12] R. Islam, C. Senko, W. C. Campbell, S. Korenblit, J. Smith, A. Lee, E. E. Edwards, C.-C. J. Wang, J. K. Freericks, and C. Monroe, *Science* **340**, 583 (2013).
- [13] Z.-X. Gong, M. Foss-Feig, S. Michalakis, and A. V. Gorshkov, *Phys. Rev. Lett.* **113** (2014).
- [14] M. Foss-Feig, Z.-X. Gong, C. W. Clark, and A. V. Gorshkov, *Phys. Rev. Lett.* **114** (2015).
- [15] M. P. Zaletel, R. S. K. Mong, C. Karrasch, J. E. Moore, and F. Pollmann, *Phys. Rev. B* **91**, 165112 (2015).
- [16] S. Choi, J. Choi, R. Landig, G. Kucsko, H. Zhou, J. Isoya, F. Jelezko, S. Onoda, H. Sumiya, V. Khemani, C. von Keyserlingk, N. Y. Yao, E. Demler, and M. D. Lukin, *Nature (London)* **543**, 221 (2017).
- [17] M. Gärtner, J. G. Bohnet, A. Safavi-Naini, M. L. Wall, J. J. Bollinger, and A. M. Rey, *Nat. Phys.* **13**, 781 (2017).
- [18] X. Chen and T. Zhou, *Phys. Rev. B* **100**, 064305 (2019).
- [19] M. C. Tran, A. Y. Guo, Y. Su, J. R. Garrison, Z. Eldredge, M. Foss-Feig, A. M. Childs, and A. V. Gorshkov, *Phys. Rev. X* **9**, 031006 (2019).
- [20] C.-F. Chen and A. Lucas, *Phys. Rev. Lett.* **123**, 250605 (2019).
- [21] D. J. Luitz and Y. B. Lev, *Phys. Rev. A* **99**, 010105(R) (2019).
- [22] S. Xu and B. Swingle, *Nat. Phys.* **16**, 199 (2020).
- [23] V. Khemani, D. A. Huse, and A. Nahum, *Phys. Rev. B* **98**, 144304 (2018).
- [24] T. Zhou and X. Chen, *Phys. Rev. E* **99**, 052212 (2019).
- [25] A. I. Larkin and Y. N. Ovchinnikov, *Sov. J. Exp. Theor. Phys.* **28**, 1200 (1969).
- [26] A. Kitaev, KITP (2015), <http://online.kitp.ucsb.edu/online/entangled15/kitaev/>.
- [27] J. Maldacena, S. H. Shenker, and D. Stanford, *J. High Energy Phys.* **08** (2016) 106.
- [28] B. Swingle, G. Bentsen, M. Schleier-Smith, and P. Hayden, *Phys. Rev. A* **94**, 040302(R) (2016).
- [29] G. Zhu, M. Hafezi, and T. Grover, *Phys. Rev. A* **94**, 062329 (2016).
- [30] N. Yunger Halpern, *Phys. Rev. A* **95**, 012120 (2017).
- [31] N. Yunger Halpern, B. Swingle, and J. Dressel, *Phys. Rev. A* **97**, 042105 (2018).
- [32] M. Campisi and J. Goold, *Phys. Rev. E* **95**, 062127 (2017).
- [33] M. Gärtner, J. G. Bohnet, A. Safavi-Naini, M. L. Wall, J. J. Bollinger, and A. M. Rey, *Nat. Phys.* **13**, 781 (2017).
- [34] K. X. Wei, C. Ramanathan, and P. Cappellaro, *Phys. Rev. Lett.* **120**, 070501 (2018).

- [35] J. Li, R. Fan, H. Wang, B. Ye, B. Zeng, H. Zhai, X. Peng, and J. Du, *Phys. Rev. X* **7**, 031011 (2017).
- [36] K. A. Landsman, C. Figgatt, T. Schuster, N. M. Linke, B. Yoshida, N. Y. Yao, and C. Monroe, *Nature (London)* **567**, 61 (2019).
- [37] N. Y. Yao, F. Grusdt, B. Swingle, M. D. Lukin, D. M. Stamper-Kurn, J. E. Moore, and E. A. Demler, [arXiv:1607.01801](https://arxiv.org/abs/1607.01801).
- [38] B. Yoshida and A. Kitaev, [arXiv:1710.03363](https://arxiv.org/abs/1710.03363).
- [39] E. J. Meier, J. Ang'ong'a, F. A. An, and B. Gadway, *Phys. Rev. A* **100**, 013623 (2019).
- [40] C. M. Sanchez, A. K. Chattah, K. X. Wei, L. Buljubasich, P. Cappellaro, and H. M. Pastawski, *Phys. Rev. Lett.* **124**, 030601 (2020).
- [41] T. Pichler, M. Dalmonte, E. Rico, P. Zoller, and S. Montangero, *Phys. Rev. X* **6**, 011023 (2016).
- [42] C. J. Turner, A. A. Michailidis, D. A. Abanin, M. Serbyn, and Z. Papić, *Nat. Phys.* **14**, 745 (2018).
- [43] J. Haegeman, J. I. Cirac, T. J. Osborne, I. Pižorn, H. Verschelde, and F. Verstraete, *Phys. Rev. Lett.* **107**, 070601 (2011).
- [44] J. Haegeman, C. Lubich, I. Oseledets, B. Vandereycken, and F. Verstraete, *Phys. Rev. B* **94**, 165116 (2016).
- [45] T. Koffel, M. Lewenstein, and L. Tagliacozzo, *Phys. Rev. Lett.* **109**, 267203 (2012).
- [46] P. Hauke and L. Tagliacozzo, *Phys. Rev. Lett.* **111**, 207202 (2013).
- [47] J. C. Halimeh and V. Zauner-Stauber, *Phys. Rev. B* **96**, 134427 (2017).
- [48] S. Chatterjee and P. S. Dey, [arXiv:1309.5757](https://arxiv.org/abs/1309.5757).
- [49] O. Hallatschek and D. S. Fisher, *Proc. Natl. Acad. Sci. U.S.A.* **111**, E4911 (2014).
- [50] V. Khemani, A. Vishwanath, and D. A. Huse, *Phys. Rev. X* **8**, 031057 (2018).
- [51] A. Nahum, S. Vijay, and J. Haah, *Phys. Rev. X* **8**, 021014 (2018).
- [52] T. Rakovszky, F. Pollmann, and C. W. von Keyserlingk, *Phys. Rev. X* **8**, 031058 (2018).
- [53] C. W. von Keyserlingk, T. Rakovszky, F. Pollmann, and S. L. Sondhi, *Phys. Rev. X* **8**, 021013 (2018).
- [54] S. Xu and B. Swingle, *Phys. Rev. X* **9**, 031048 (2019).
- [55] S. Sachdev and J. Ye, *Phys. Rev. Lett.* **70**, 3339 (1993).
- [56] D. A. Roberts, D. Stanford, and A. Streicher, *J. High Energy Phys.* **06** (2018) 122.
- [57] I. Calvo, J. C. Cuchi, J. G. Esteve, and F. Falceto, *J. Stat. Phys.* **141**, 409 (2010).
- [58] S. Janson, [arXiv:1112.0220](https://arxiv.org/abs/1112.0220).
- [59] A. V. Chechkin, R. Metzler, J. Klafter, and V. Y. Gonchar, in *Anomalous Transport* (John Wiley & Sons, Ltd, Wiley, 2008), pp. 129–162.
- [60] See the Supplemental Material at <http://link.aps.org/supplemental/10.1103/PhysRevLett.124.180601> for more details.
- [61] E. Leviatan, F. Pollmann, J. H. Bardarson, D. A. Huse, and E. Altman, [arXiv:1702.08894](https://arxiv.org/abs/1702.08894).